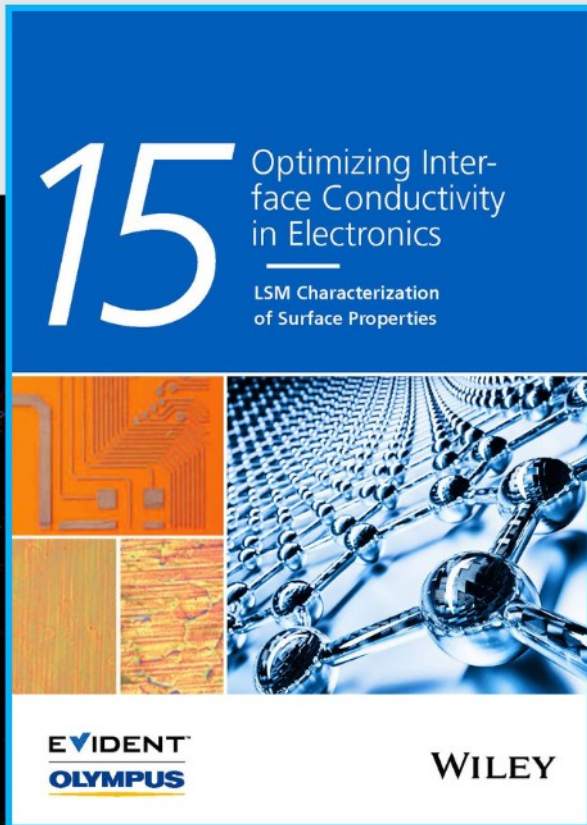| Title	Half-Metallic Heusler Alloy/GaN Heterostructure for Semiconductor Spintronics Devices
Author(s)	Yamada, Shinya; Kato, Masatoshi; Ichikawa, Shuhei et al.
Citation	Advanced Electronic Materials. 2023, 9(7), p. 2300045
Version Type	VoR
URL	https://hdl.handle.net/11094/92488
rights	This article is licensed under a Creative Commons Attribution 4.0 International License.
Note	

Half-Metallic Heusler Alloy/GaN Heterostructure for Semiconductor Spintronics Devices

Shinya Yamada,* Masatoshi Kato, Shuhei Ichikawa, Michihiro Yamada, Takahiro Naito, Yasufumi Fujiwara, and Kohei Hamaya*

Because spin-orbit coupling in wurtzite semiconductors is relatively weak compared with that in zincblende ones, the III-nitride semiconductor GaN is a promising material for high-performance optical semiconductor spintronic devices such as spin lasers. For the purpose of reducing the operating power of spin lasers, it is necessary to demonstrate highly efficient electrical spin injection from a ferromagnetic material into GaN with a low-resistance contact. Here, an epitaxial half-metallic Heusler alloy $Co_2FeAl_xSi_{1-x}$(CFAS)/GaN heterostructure is developed by inserting an ultrathin Co layer between the CFAS and GaN. The CFAS/n^+-GaN heterojunctions clearly show tunnel conduction with very small rectification and a low resistance-area product of ≈ 3.8 kΩµm^2, which is several orders of magnitude smaller than those reported in previous work, at room temperature. Nonlocal spin signals and a Hanle effect curve are observed at low temperatures using lateral spin-valve devices with the CFAS/n^+-GaN contacts, suggesting pure spin current transport in bulk GaN. The spin transport is observed at temperatures as high as room temperature, with a high spin polarization of 0.2 at a low bias voltage less than 2.0 V. This study is expected to open a path to GaN-based spintronic devices with highly spin-polarized and low-resistance contacts.

1. Introduction

The wide-bandgap III-nitride semiconductor GaN, which generally has the hexagonal wurtzite structure shown in **Figure 1**b, has been widely studied for use in electronic and optoelectronic devices ranging from high-electron-mobility transistors[1,2] to light-emitting diodes (LEDs).[3–6] The growth of GaN quantum dots[7,8] and GaN nanowires[7,9,10] has recently been explored for single-photon emitters in quantum information processing applications, and full-color micro-LEDs have been reported in monolithically stacked Eu-doped GaN and InGaN quantum well heterostructures.[11] Because of the intrinsically weak spin-orbit coupling in GaN,[12–14] the possibility of semiconductor spintronic devices such as a spin LED[15–17] and spin field-effect transistor[18,19] has also emerged in the field of GaN systems. Thus far, it has been demonstrated,

S. Yamada, M. Kato, M. Yamada, T. Naito, K. Hamaya
Center for Spintronics Research Network
Graduate School of Engineering Science
Osaka University
1-3 Machikaneyama, Toyonaka, Osaka 560-8531, Japan
E-mail: yamada.shinya.es@osaka-u.ac.jp;
hamaya.kohei.es@osaka-u.ac.jp

S. Yamada, K. Hamaya
Department of Systems Innovation
Graduate School of Engineering Science
Osaka University
1-3 Machikaneyama, Toyonaka, Osaka 560-8531, Japan

S. Yamada, Y. Fujiwara, K. Hamaya
Spintronics Research Network Division
Institute for Open and Transdisciplinary Research Initiatives
Osaka University
2-1 Yamadaoka, Suita, Osaka 565-0871, Japan

S. Ichikawa
Division of Electrical, Electronic and Infocommunications Engineering
Graduate School of Engineering
Osaka University
2-1 Yamadaoka, Suita, Osaka 565-0871, Japan

M. Yamada
PRESTO
Japan Science and Technology Agency
4-1-8 Honcho, Kawaguchi, Saitama 332-0012, Japan

Y. Fujiwara
Division of Materials and Manufacturing Science
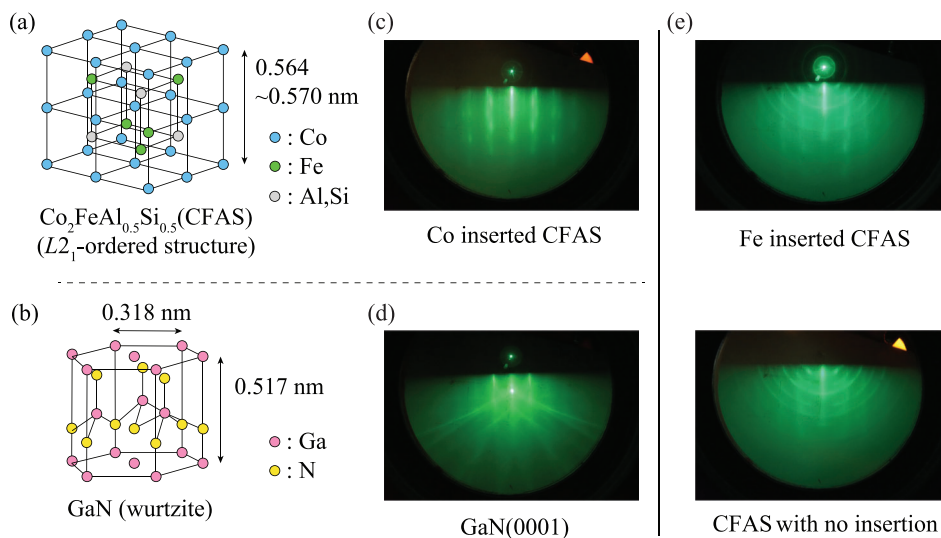Graduate School of Engineering
Osaka University
2-1 Yamadaoka, Suita, Osaka 565-0871, Japan

Figure 1. Crystal structure of a) $L2_1$-type Heusler alloy and b) wurtzite-type GaN. RHEED images for the $Co_2FeAl_xSi_{1-x}$ layer for the c) Co-insertion, e) Fe-insertion and no-insertion surfaces, and d) surface of GaN(0001) before growth. All patterns were recorded with an incident electron beam along the GaN[11$\bar{2}$0] direction.

even at room temperature, electrical spin injection into GaN in LED structures [20–23] and three- or four-terminal lateral device structures.[23–29] However, almost all of the previous related studies have used an insulating tunnel barrier such as MgO and AlN for electrical spin injection into GaN to solve the spin resistance mismatch problem,[30–32] resulting in high-resistance contacts with a resistance-area product (*RA*) higher than several MΩμm^2.[20,21,29] If such high-resistance contacts were utilized, they would limit the future use of GaN in applications such as medical spin LEDs,[33] and spin-polarized lasers (spin lasers) for ultrafast switches, high-performance reconfigurable interconnects, and secure communications on chips.[34–37] Although a spin laser was experimentally demonstrated in a GaN-nanorod array coupled with Fe_2O_3 nanoparticles at room temperature in 2014,[38] spin injection was performed by optical pumping with circularly polarized light, giving rise to an obstruction for on-chip battery-operated devices. Therefore, highly efficient electrical spin injection from a ferromagnetic material into GaN with a low-resistance contact should be explored.

To achieve room-temperature electrical spin injection into III-V GaAs and group-IV Ge semiconductors without using an insulating tunnel barrier, half-metallic Heusler alloy/semiconductor Schottky tunnel contacts have been investigated.[39–42] Co-based Heusler alloys have the chemical formula Co_2YZ, where *Y* is a transition metal and *Z* is a main-group element, are candidate materials for half-metals with a fully spin-polarized density of states at the Fermi level.[43–47] As a result, certain half-metallic Co_2YZ alloys with an $L2_1$-ordered structure (Figure 1a) can solve the spin resistance mismatch problem.[40–42] Because GaAs and Ge also have cubic lattice structures known as zincblende and diamond structures, respectively, there was good matching between the atomic arrangements of the half-metallic Co_2YZ alloys and GaAs or Ge.[42] Also, there was almost no lattice mismatch (less than 1%) between some of the half-metallic Heusler alloys (0.564–0.570 nm)[42] and GaAs or Ge (0.566 nm). Thus, high-quality epitaxial half-metallic Co_2YZ/GaAs[40] or half-metallic

Co_2YZ/Ge heterostructures[41,42,48] have been experimentally obtained, resulting in highly efficient spin injection even at room temperature. However, the crystal structure of wurtzite-type GaN is completely different from that of $L2_1$-type Co_2YZ Heusler alloys, and there is no matching between the lattice length and symmetry, as shown in Figure 1b. Thus far, although studies on the growth of ferromagnetic metals such as Fe[49–51] and Co[52] on GaN and on the electrical properties of epitaxial Fe/GaN(0001) Schottky tunnel contacts[53] have been reported, $L2_1$-type Co_2YZ Heusler alloy/GaN heterostructures have not been developed for semiconductor spintronic applications.

Here, we experimentally achieve epitaxial growth of cubic $Co_2FeAl_xSi_{1-x}$ (CFAS) films with an $L2_1$-ordered structure on wurtzite GaN(0001) by inserting an ultrathin Co layer between CFAS and GaN. Using a heavily doped n^+-GaN layer, we demonstrate tunnel conduction with very small rectification and a low *RA* of 3.8 kΩμm^2, which is several orders of magnitude smaller than the values reported in previous works, at room temperature. For lateral spin-value devices with the developed CFAS/n^+-GaN tunnel contacts, we clearly observe nonlocal spin signals and a Hanle-effect curve at 100 K, which is clear evidence for the generation, manipulation, and detection of pure spin currents in the n^+-GaN layer. The pure spin current transport is observed up to room temperature with a high spin polarization of 0.2 at a bias voltage of less than 2.0 V even at room temperature. We expect the results of this study to open a path to the development of GaN-based spintronic devices with highly spin-polarized and low-resistance contacts.

2. Experimental Section

2.1. Growth of CFAS Films on GaN

To obtain a GaN(0001) surface, 1.4-μm-thick undoped GaN layers were epitaxially grown on commercial Al_2O_3(0001) substrates by metal-organic vapor phase epitaxy.[5,11] We then chemically

**ADVANCED
SCIENCE NEWS**

www.advancedsciencenews.com

**ADVANCED
ELECTRONIC
MATERIALS**

www.advelectronicmat.de

cleaned the surface of the epitaxial GaN layer with a 1% HF solution to remove the native oxide and contamination, and subsequently loaded the sample into a molecular beam epitaxy (MBE) chamber with a base pressure of $\approx 10^{-7}$ Pa. To grow a Co-based Heusler alloy, CFAS, the supply of atoms was intentionally controlled under the nonstoichiometric condition, where the ratio of Co, Fe, Al, and Si was set to 1.8 : 1 : 1 : 0.5,[54,55] using Knudsen cells in an MBE system. The growth temperature for the CFAS layer was 300 °C. Notably, for the spin-transport GaN layer, a ≈ 135 nm-thick n^+-GaN layer was grown on a ≈ 1.4 μm-thick un-doped GaN layer on a commercial Al_2O_3 (0001) substrate. The carrier concentration (n) in the n^+-GaN layers was $\approx 5 \times 10^{19}$ cm^{-3} at 300 K, as estimated from Hall-effect measurements. The Schottky barrier height (ϕ_B) for the CFAS/n-GaN contact was estimated to be ≈ 0.8 eV from current-voltage characteristics of CFAS/n-GaN Schottky diodes.

2.2. Fabrication of Lateral Spin-Valve Devices

Lateral spin-valve (LSV) devices with CFAS/GaN Schottky tunnel contacts were fabricated by microfabrication techniques. As the spin injector and detector contacts, two different CFAS/n^+-GaN contacts with areas of 2 μm^2 and 5 μm^2 by electron-beam lithography, Ar-ion milling, and inductively coupled plasma reactive-ion etching (ICP-RIE) with Cl$_2$ were defined.[11,56,57] Here, the CFAS layer was removed by Ar-ion milling and the damaged n^+-GaN surface was subsequently removed by ICP-RIE. To obtain different switching fields and stable antiparallel magnetization states, the pointed end shape was used for smaller ferromagnetic contacts. The sizes of the CFAS/n^+-GaN contacts were 0.4 × 5.0 μm^2 and 1.0 × 5.0 μm^2, and the edge-to-edge distances (d) between the CFAS/n^+-GaN contacts were designed to be 0.5-0.7 μm. Because they were completely covered by the 100 nm-thick SiO$_2$ insulating layer, the CFAS/n^+-GaN contacts were simply connected to the n^+-GaN spin-transport layer with the area of these CFAS/n^+-GaN contacts. Thus, there was no leakage current from the large Au/Ti contact pads to the n^+-GaN spin-transport layer in all the measurements conducted in the present work.

2.3. Characterization

Structural characterizations were carried out using in situ reflection high-energy electron diffraction (RHEED) observations, X-ray diffraction (XRD), high-angle annular dark-field scanning transmission electron microscopy (HAADF-STEM) and energy-dispersive X-ray spectroscopy (EDX) measurements. Magnetic properties were measured using a vibrating sample magnetometer in a physical property measurement system (Quantum Design). Nonlocal spin-valve measurements were carried out by a conventional direct current-bias technique (approximately −1.5 mA) at various temperatures in a cryostat. We controlled the magnetization configuration between parallel and anti-parallel states of the spin injector and detector by adjusting the external magnetic field B, where B was applied along the long axis of the CFAS/n^+-GaN contacts.

3. Results and Discussion

3.1. Half-Metallic CFAS on GaN

To solve the spin resistance mismatch problem between ferromagnetic metals and GaN,[30–32] it is very important to utilize a Schottky-tunnel barrier with half-metallic spin injector and detector,[39–42] as described in section I. Furthermore, if we need to use a Co-based Heusler alloy as a theoretically expected half-metallic material, we should obtain the $L2_1$-type structure even on GaN. Thus, to realize $L2_1$-ordered CFAS/GaN heterostructures for highly efficient spin injection through the Schottky-tunnel interface, we explore the effect of ultrathin atomic layer insertion on the crystal growth of CFAS films on GaN(0001). First, we confirm a good flatness of the GaN(0001) surface by in situ RHEED observations in Figure 1d. We then focus on hexagonal close-packed (hcp)-type Co as an insertion element between CFAS and GaN(0001). Like the wurtzite-type GaN(0001) surface, the hcp-type Co(0001) surface has a hexagonal atomic arrangement. Although a large lattice mismatch of $\approx 24\%$ exists between Co(0001) (≈ 0.251 nm) and GaN(0001) (≈ 0.318 nm), epitaxial growth of Co films on GaN(0001) has already been reported.[52] After we deposited a ≈ 0.4 nm-thick Co layer onto GaN(0001) at 300 °C, we grew a ≈ 30 nm-thick CFAS film on the surface at the same substrate temperature (see Section 2.1).[54,55] Notably, we can clearly see a streak pattern of the RHEED image (Figure 1c), indicating 2D epitaxial growth of the CFAS film on GaN(0001). To check the effect of the ≈ 0.4-nm-thick Co layer insertion, we also grew CFAS films by inserting a ≈ 0.3-nm-thick Fe layer, where the crystal structure of Fe is body-centered cubic, in addition to growth without an insertion layer. Consequently, the RHEED images include a ring-like pattern in addition to the streaks, as shown in Figure 1e, for the Fe-insertion and no-insertion surfaces, indicating that the grown CFAS films are composed of polycrystalline phases. Therefore, the insertion of an ultra-thin Co layer is necessary to obtain epitaxial CFAS films on GaN(0001). In the following discussion, we refer to epitaxial CFAS/Co/GaN/Al$_2$O$_3$(0001) heterostructures as CFAS/GaN for simplicity.

Figure 2a shows an ω-2θ XRD pattern for the CFAS/GaN(0001) heterostructures. First, 220 diffraction peak for CFAS is clearly observed. The lattice constant is estimated to be ≈ 0.567 nm, approximately equivalent to that for bulk-CFAS (≈ 0.568 nm).[58] Except for the diffraction peaks derived from the GaN/Al$_2$O$_3$(0001) substrates, no peaks originating from other phases are observed. These results indicate that the (110)-oriented epitaxial CFAS film is demonstrated on GaN(0001). To further investigate the in-plane epitaxial relationship for the CFAS/GaN(0001) heterostructures, we perform ϕ-scan measurements for the (220) planes of the CFAS film (Figure 2b). Six-fold symmetrical diffraction peaks are observed, however, each peak exhibits triplet splitting with an angle of $\approx 10.5°$. From the six-fold symmetry, we interpret that the (110)-oriented CFAS film is rotated in the film plane by an angle of 120°, as shown in Figure 2d. A similar epitaxial relationship has been observed for epitaxial Fe/GaN(0001) heterostructures.[49–51] In the present work, the insertion of the 0.3 nm-thick Fe layer did not lead to the 2D epitaxial growth of CFAS on GaN(0001) (Figure 1e), likely because of the surface roughness of the inserted 0.3 nm-thick Fe layer.[51] Although the mechanism for obtaining epitaxial CFAS/GaN
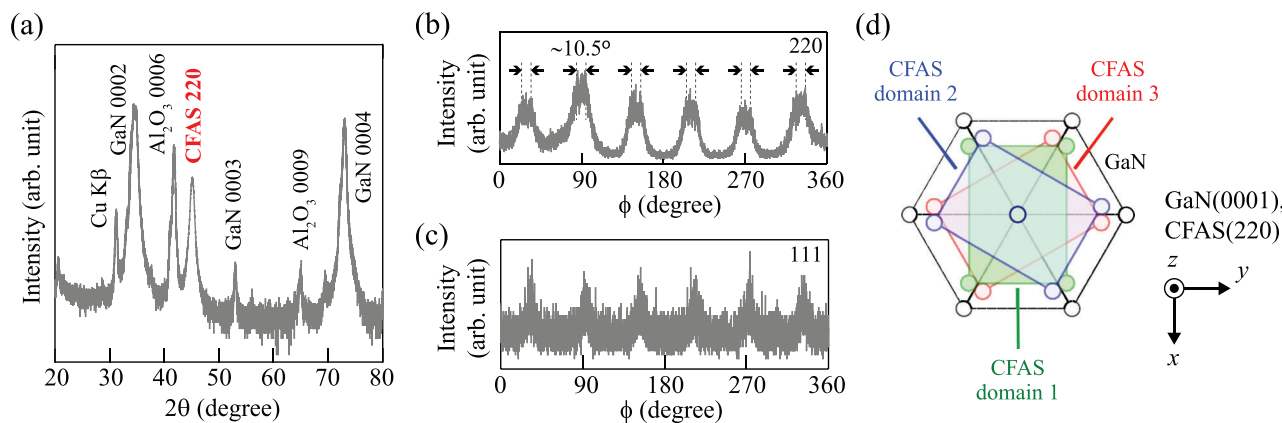
2300045 (3 of 9)

Figure 2. a) ω–2θ XRD pattern for CFAS film grown on GaN(0001). ϕ-scan measurements for the b) (220) and c) (111) planes of the CFAS film. d) Schematic (top view) of epitaxial relationship between CFAS(110) and GaN(0001).
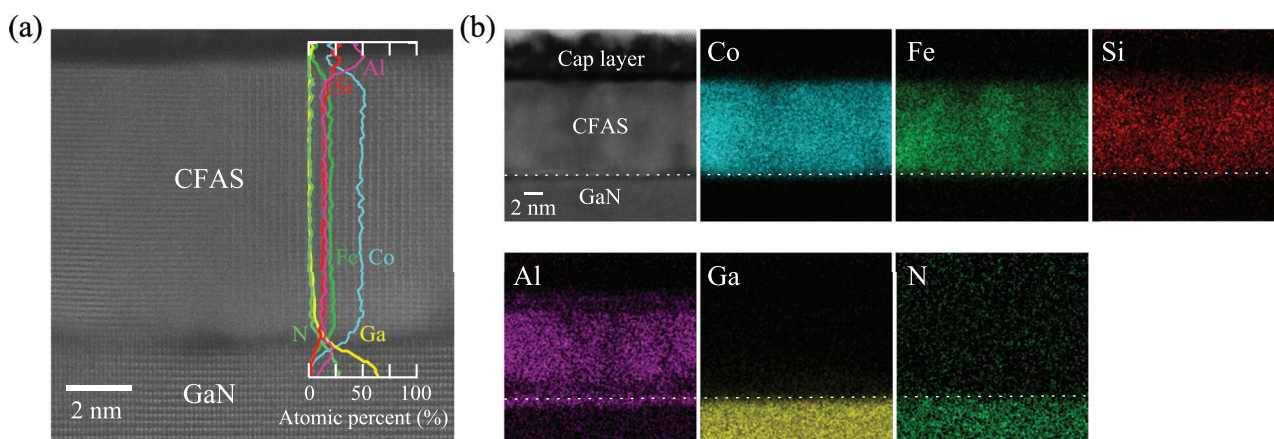

Figure 3. a) High-resolution HAADF-STEM image of epitaxial CFAS(110)/GaN(0001) heterostructure, together with EDX profile for each element. b) EDX mapping images for Co, Fe, Si, Al, Ga, and N, together with corresponding HAADF-STEM image.

heterostructure has been still unclear, we have speculated the difference in the surface quality of GaN(0001) with the metal insertion affects the crystal growth of CFAS films. If single-crystal CFAS films were grown on GaN(0001), we would expect to observe two-fold symmetrical diffraction peaks in the ϕ-scan measurement for the (220) plane. Thus, the 120° in-plane-rotated growth of the CFAS film implies the epitaxial growth close to the Nishiyama-Wassermann orientation relationship, CFAS[001](110)//GaN[11$\bar{2}$0](0001). An XRD ϕ-scan measurement for the (111) planes of the CFAS film is shown in Figure 2c, where the 111 peak represents superlattice diffraction from $L2_1$-ordered Co_2YZ. We thus observe diffraction peaks because of the presence of the $L2_1$-ordered structures in the CFAS film. From these XRD measurements, (110)-oriented epitaxial CFAS films including the $L2_1$-ordered structure are demonstrated even on GaN(0001).

We also perform HAADF-STEM observations and EDX measurements. **Figure 3**a shows a high-resolution HAADF-STEM image, together with an EDX line profile, for the epitaxial CFAS/GaN heterojunction. The dark lattice image within 1 nm of the CFAS/GaN(0001) heterointerface indicates that lattice distortion and/or relaxation due to a very large lattice mismatch ($\approx$24%) between the inserted Co and GaN is induced at the CFAS/GaN

interface. Because the thickness of the Co insertion layer is very thin (0.4 nm), it is difficult to get information on the Co layer from the HAADF-STEM image. The lattice image of the epitaxial CFAS layer looks no good probably due to the in-plane-rotated growth of the CFAS layer on GaN. Figure 3b displays EDX elemental maps for Co, Fe, Si, Al, Ga, and N. Slight diffusion of Al toward the heterointerface within 1 nm is observed. Because the growth temperature for the CFAS film on GaN(0001) in the present study is 300 °C, which is higher than those on Si(111) or Ge(111) in our previous studies (room temperature),[54,55] slight diffusion of Al toward the GaN layer is promoted, leading to the unintentional formation of an ultrathin Al-doped GaN (or Al-GaN) layer at the CFAS/GaN heterointerface. Here, we can expect little effect of the formed layer on the spin injection and detection because the ultrathin Al-doped GaN (or AlGaN) layer becomes an appropriate tunnel barrier layer with a low contact resistance.[29]

Figure 4 shows the magnetic-field dependence of the magnetization (M–H curve) for an epitaxial CFAS/GaN heterostructure at room temperature (300 K). The saturation magnetic moment (M_S) is estimated to be $\approx$4.7 μ_B/f.u., which is equivalent to the M_S values for the CFAS films grown on a Si(111) or Ge(111) substrate in our previous studies.[54,55] Although the value of M_S is slightly smaller than that for bulk CFAS,[58] the coercivity is
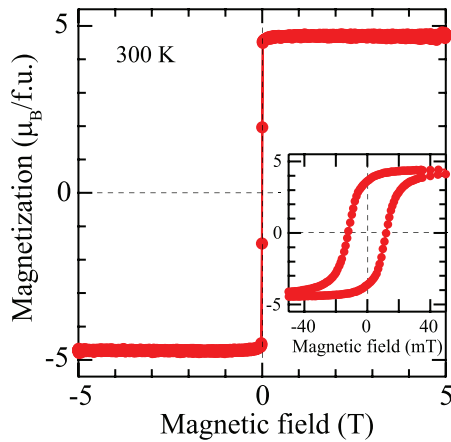
2300045 (4 of 9)

**ADVANCED
SCIENCE NEWS**

www.advancedsciencenews.com

**ADVANCED
ELECTRONIC
MATERIALS**
Open Access

www.advelectronicmat.de

Figure 4. High-field M–H curve for an epitaxial CFAS film measured along [11$\bar{2}$0] direction at 300 K. The inset shows a low-field M–H curve.

equivalent to that for CFAS/Ge(111),[55] as shown in the inset. The epitaxial CFAS/GaN heterostructure is expected to be used as a highly efficient spin injector.[41,42,55] These structural and magnetic characterizations show that sufficiently high-quality $L2_1$-ordered CFAS/GaN heterostructures were realized by inserting an ultrathin Co layer between the CFAS and the GaN(0001) surface during growth. Therefore, we can use the $L2_1$-ordered CFAS/GaN heterostructures as a Schottky-tunnel-type spin injector for highly efficient spin injection into GaN.

3.2. Spin Transport in GaN

In the previous section, we have developed an $L2_1$-ordered CFAS/GaN heterostructure that can overcome the spin resistance mismatch problem.[30–32] A schematic of the fabricated lateral spin-valve (LSV) device with CFAS/GaN contacts is presented in **Figure 5**a, where the GaN is a heavily Si-doped GaN layer (n^+-GaN; ≈5 × 10^{19} cm^{-3} at 300 K) to promote tunnel conduction at the CFAS/GaN heterojunction. A representative fabricated LSV device is shown in Figure 5b. The LSV device has two CFAS/n^+-GaN contacts for spin injection and detection, and two Au/Ti ohmic contacts are formed at the ends of the n^+-GaN layer.[24,28] The two-different shaped CFAS/GaN contacts (FM1 and FM2) were also connected to Au/Ti bonding pads to measure the spin transport through the n^+-GaN layer. Before the spin-transport measurements, we confirmed the current–voltage (I–V) characteristics of the CFAS/n^+-GaN interfaces, as presented in Figure 5c, at 50–300 K. Here, the I–V characteristics of the CFAS/n^+-GaN interface were evaluated by three-terminal methods, as illustrated in the inset. Because of the use of the heavily doped GaN layer, the I–V characteristics of the CFAS/n^+-GaN interface exhibit small rectifying behavior even at low temperatures, indicating that tunnel conduction of electrons for electrical spin injection from the CFAS layer into the n^+-GaN channel is dominant. These results indicate that we obtained CFAS/n^+-GaN Schottky tunnel-like contacts with an RA of ≈3.8 kΩμm^2. This value is six or seven orders of magnitude smaller than that for CoFe/MgO/GaN devices.[26] This smaller RA value is a significant advantage of the CFAS/n^+-GaN Schottky tunnel-like contacts without an oxide insulating tunnel barrier over the

CoFe/MgO/GaN contacts. Here, the RA of ≈3.8 kΩμm^2 is still large to sufficiently suppress the spin absorption from n^+-GaN into CFAS. In our measurements, the negative sign of I ($I < 0$) indicates that the spin-polarized electrons are injected from the CFAS into the n^+-GaN, that is, under the spin injection condition through the Schottky tunnel barrier with a Schottky barrier height of ≈0.8 eV, as shown in Figure 5d.

By applying in-plane magnetic fields along the y direction (B_y), we conducted nonlocal voltage measurements.[59–61] **Figure 6**a shows a representative nonlocal spin signal ($\Delta R_{NL} = \Delta V_{NL}/I$) at $I = -1.5$ mA at 100 K. A spin-valve-like signal with a magnitude of ≈17 mΩ is clearly observed. This spin-valve behavior is attributed to the change in the magnetization states between parallel and antiparallel for the two-different shaped CFAS/GaN contacts (FM1 and FM2), as depicted in the inset. To measure the nonlocal Hanle effect, we recorded ΔR_{NL} by applying out-of-plane magnetic fields along the z direction (B_z) under the parallel magnetization state at 100 K (Figure 6b). With increasing $|B_z|$, the value of ΔR_{NL} is reduced, indicating precessional decay of the spin polarization in the n^+-GaN layer. These features provide evidence for the generation, manipulation, and detection of pure spin currents in the n^+-GaN layer. Therefore, the data in Figure 6a,b represents the first experimental demonstration of pure spin current transport in n^+-GaN through half-metallic Heusler alloy/n^+-GaN contacts with a low RA value.

Using the Hanle effect curve in Figure 6b, we can roughly extract the spin lifetime (τ_{GaN}) in n^+-GaN. According to previous works,[61] the nonlocal Hanle effect curve with the parallel magnetization state ($\uparrow\uparrow$) is expressed using the following 1D spin drift-diffusion model:

$$\Delta R_{NL(\uparrow\uparrow)}(B_z) = +\frac{P^2 \rho_{GaN} D}{S} \int_0^\infty \frac{1}{\sqrt{4\pi Dt}} \exp\left(-\frac{d^2}{4Dt}\right)$$

$$\times \cos(\omega_L t)\exp\left(-\frac{t}{\tau_{GaN}}\right)dt \qquad (1)$$

where D is the diffusion constant for the n^+-GaN layer, (≈12.7 cm^2/s), ω_L (= $g\mu_B B_z/\hbar$) is the Larmor frequency, g is the electron g-factor ($g \approx 2$)[62–65] in GaN, and μ_B is the Bohr magneton. P is the electron spin polarization in n^+-GaN created by the CFAS. Here, for our GaN-based LSV devices, d and S are the edge-to-edge distances between the CFAS/n^+-GaN contacts, as shown in Figure 5a, and the cross-section area of the n^+-GaN layer, respectively. ρ_{GaN} is the electrical resistivity of the n^+-GaN layer (≈7.6 Ωμm). The solid black curve in Figure 6b indicates the results of fitting using Equation (1). From the results, τ_{GaN} and D are estimated to be ≈62 ps and ≈12.7 cm^2 s^{-1}, respectively. This value of τ_{GaN} is consistent with those reported for highly degenerate n-GaN, that is, n^+-GaN (≈10^{19} cm^{-3}) measured by time-resolved Kerr rotation spectroscopy.[66] Using the relation $\lambda_{GaN} = \sqrt{D\tau_{GaN}}$, we obtain a λ_{GaN} value of ≈ 280 nm at 100 K, where λ_{GaN} is the spin diffusion length for the n^+-GaN layer. Given this situation, we can also expect the value of τ_{GaN} at room temperature to be 28–55 ps.[66]

From the results of fitting using Equation (1), we also obtain a spin polarization P of ≈0.25 (100 K) created in the n^+-GaN layer. The value of P at 100 K is similar to that for an LSV device with CFAS/Ge Schottky tunnel contacts,[67] where the CFAS/Ge
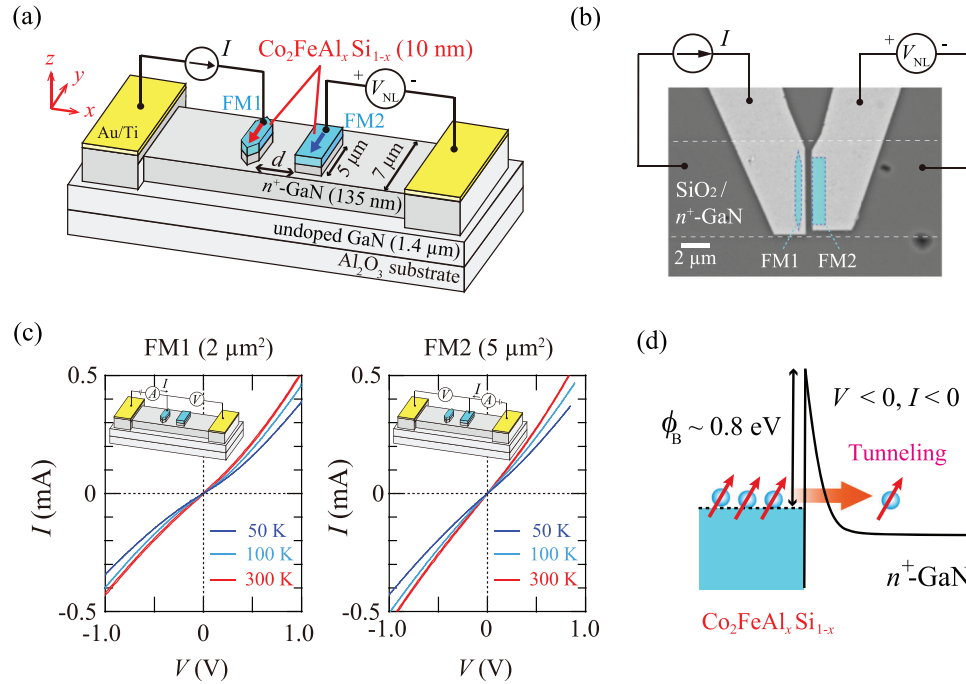
Figure 5. a) Schematic and b) SEM image (top view) of a lateral spin-valve (LSV) device fabricated with CFAS/n^+-GaN Schottky-tunnel contacts. c) I–V characteristics for CFAS/n^+-GaN contacts measured at 50–300 K. d) Schematic of spin injection through CFAS/n^+-GaN Schottky-tunnel barrier.
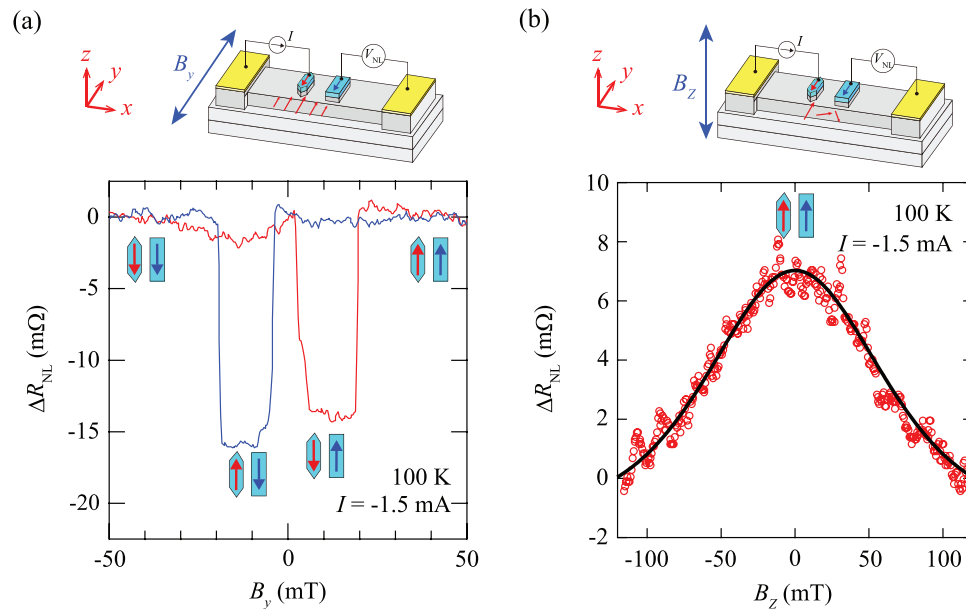

Figure 6. a) Nonlocal spin signal versus in-plane magnetic field and b) nonlocal Hanle effect curve under parallel magnetization state versus an out-of-plane magnetic field at 100 K at $I = -1.5$ μA for LSV device with $d = 0.7$ μm.

Schottky tunnel contacts are a highly efficient spin injector and detector for Ge. In general, the value of ΔR_{NL} can also be expressed by the following equation:[61]

$$|\Delta R_{NL}| = \frac{P^2 \rho_{GaN} \lambda_{GaN}}{S} \exp\left(-\frac{d}{\lambda_{GaN}}\right) \qquad (2)$$

Using this relation, we also obtain $P \approx 0.27$, roughly consistent with the value ($P \approx 0.25$) estimated by fitting using Equation (1). Therefore, highly efficient spin injection from CFAS into n^+-GaN through the low-resistance junctions is reliably demonstrated at 100 K. We believe that the solution of the spin resistance mismatch problem between ferromagnetic metal and GaN is experimentally shown in this study. In our previous work on the
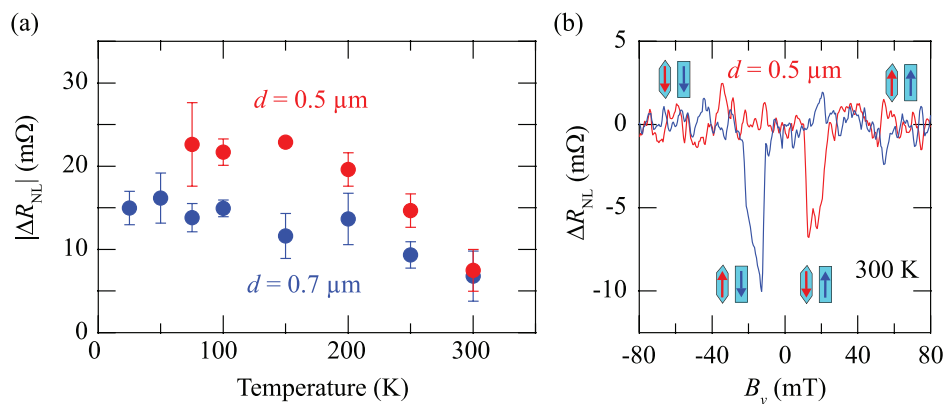
**ADVANCED
SCIENCE NEWS**

www.advancedsciencenews.com

**ADVANCED
ELECTRONIC
MATERIALS**

www.advelectronicmat.de

Figure 7. a) Temperature dependence of magnitude of nonlocal spin signals, $|\Delta R_{NL}|$, for various LSV devices. b) Representative nonlocal spin signal measured at room temperature.

epitaxial and $L2_1$-ordered CFAS/Ge,[41] we found that the thickness of the insertion layer between CFAS and Ge affects the efficiency of the electrical spin injection. In the present study, we used a 0.4-nm-thick Co insertion layer for the epitaxial growth of $L2_1$-ordered CFAS on GaN(0001). In future work, we will further investigate the effect of the thickness of the Co insertion layer between CFAS and GaN on the efficiency of the electrical spin injection.

3.3. Spin Polarization at Room Temperature

We finally explore the possibility of room-temperature operation of GaN-based spintronic devices. **Figure 7**a shows the temperature dependence of $|\Delta R_{NL}|$ for LSV devices with $d = 0.5$ (red) and 0.7 (blue) µm. For both devices, a relatively large temperature dependence is observed above 150 K. Notably, nonlocal spin signals are observed even at 300 K (room temperature), as shown in Figure 7b. This means that room-temperature pure spin-current transport in a bulk GaN layer is detected via the CFAS/n^+-GaN interfaces without using an oxide insulating tunnel barrier. Room-temperature spin transport was detected at a bias voltage of less than $\approx$2.0 V at the CFAS/n^+-GaN contacts.

We can evaluate the value of P at 300 K by substituting appropriate experimental parameters and the expected λ_{GaN} value at room temperature in Equation (2). According to the estimated value of D ($\approx$16.2 cm²s⁻¹) and a reliable τ_{GaN} ($\approx$ 45 ps) value at room temperature,[66] we roughly estimate λ_{GaN} at 300 K as $\approx$270 nm. As a result, we extract $P \approx 0.24$ from Equation (2). In a previous study on a spin laser consisting of a CoFe/MgO/GaN-diode structure,[21] the value of P was demonstrated to range from 0.05 to 0.1 at room temperature. Our P value in the present study is twice as large as those reported in previous works, implying the feasibility of a spin laser with an $L2_1$-ordered CFAS/n^+-GaN contact.

We here comment on the low-power operation of a spin laser with an $L2_1$-ordered CFAS/n^+-GaN contact. In a previous CoFe/MgO/GaN-diode structure,[21] laser operation was performed at large bias voltages because an oxide insulating tunnel barrier was used. Assuming that the voltage applied to the CoFe/MgO/GaN contact is the same as the bias voltage applied to the diode structure, we can roughly estimate that a bias volt-

age higher than 5.0 V is required to obtain a threshold current ($\approx$19 µA) for operating the spin laser.[21] If the same injection current is needed for a laser with a CFAS/n^+-GaN contact, a bias voltage of only $\approx$ 0.05 V is expected, which is two orders of magnitude smaller than the bias voltage with the CoFe/MgO/GaN contact. As mentioned, the value of P for our CFAS/n^+-GaN devices is approximately twice as large as those for CoFe/MgO/GaN-diode structures.[21] Here, since the CoFe is not a half-metal and CoFe/MgO is not oriented along 001, the spin injection/detection efficiency of the CoFe/MgO/GaN contacts is expected to be smaller than that of the $L2_1$-ordered CFAS/GaN ones. Therefore, we expect that a spin laser with a CFAS/n^+-GaN contact can greatly suppress electric power consumption compared with that reported in the previous work.[21]

4. Conclusion

The III-nitride semiconductor GaN is a promising material for high-performance optical semiconductor spintronic devices such as spin lasers. To realize a half-metallic material/GaN spin injector, we explored an epitaxial half-metallic Heusler alloy CFAS/GaN heterostructure by inserting an ultrathin Co layer between the CFAS and GaN. The $L2_1$-ordered CFAS/n^+-GaN heterojunctions clearly showed tunnel conduction with very small rectification and a low resistance-area product of $\approx$3.8 kΩµm², which is several orders of magnitude smaller than those reported in previous works, at room temperature. Using LSV devices with the $L2_1$-ordered CFAS/n^+-GaN contacts, we observed nonlocal spin signals and a Hanle effect curve at low temperatures, providing evidence for pure spin current transport in bulk GaN. Spin transport was observed at temperatures as high as room temperature with a high spin polarization of $\approx$0.2 at a low bias voltage less than $\approx$2.0 V. We expect the results of this study to open a path to the development of a GaN-based spin laser with highly spin-polarized and low-resistance contacts.

2300045 (7 of 9)

Conflict of Interest

The authors declare no conflict of interest.

Data Availability Statement

The data that support the findings of this study are available from the corresponding author upon reasonable request.

[1] U. K. Mishra, P. Parikh, Y.-F. Wu, *Proc. IEEE* **2002**, *90*, 1022.

[2] Y. Ando, S. Kaneki, T. Hashizume, *Appl. Phys. Express* **2019**, *12*, 024002.

[3] I. Akasaki, H. Amano, *Jpn. J. Appl. Phys.* **2006**, *45*, 9001.

[4] C.-H. Lu, C.-C. Lan, Y.-L. Lai, Y.-L. Li, C.-P. Liu, *Adv. Funct. Mater.* **2011**, *21*, 4719.

[5] B. Mitchell, V. Dierolf, T. Gregorkiewicz, Y. Fujiwara, *J. Appl. Phys.* **2018**, *123*, 160901.

[6] F. Liu, Z. Zhang, X. Rong, Y. Yu, T. Wang, B. Sheng, J. Wei, S. Zhou, X. Yang, F. Xu, Z. Qin, Y. Zhang, K. Liu, B. Shen, X. Wang, *Adv. Funct. Mater.* **2020**, *30*, 2001283.

[7] Y. Arakawa, M. J. Holmes, *Appl. Phys. Rev.* **2020**, *7*, 021309.

[8] L. Chen, B. Sheng, S. Sheng, P. Wang, X. Sun, D. Li, T. Wang, R. Tao, S. Liu, Z. Chen, W. Ge, B. Shen, X. Wan, *Adv. Funct. Mater.* **2022**, *32*, 2208340.

[9] S. Deshpande, J. Heo, A. Das, P. Bhattacharya, *Nat. Commun.* **2013**, *4*, 1675.

[10] I. Aharonovich, D. Englund, M. Toth, *Nat. Photonics* **2016**, *10*, 631.

[11] S. Ichikawa, K. Shiomi, T. Morikawa, D. Timmerman, Y. Sasaki, J. Tatebayashi, Y. Fujiwara, *Appl. Phys. Express* **2021**, *14*, 031008.

[12] B. Beschoten, E. Johnston-Halperin, D. K. Young, M. Poggio, J. E. Grimaldi, S. Keller, S. P. DenBaars, U. K. Mishra, E. L. Hu, D. D. Awschalom, *Phys. Rev. B* **2001**, *63*, 121202(R).

[13] S. Krishnamurthy, M. van Schilfgaarde, N. Newman, *Appl. Phys. Lett.* **2003**, *83*, 1761.

[14] X. Liu, N. Tang, S. Zhang, X. Zhang, H. Guan, Y. Zhang, X. Qian, Y. Ji, W. Ge, B. Shen, *Adv. Sci.* **2020**, *7*, 1903400.

[15] Y. Ohno, D. K. Young, B. Beschoten, F. Matsukura, H. Ohno, D. D. Awschalom, *Nature* **1999**, *402*, 790.

[16] B. T. Jonker, Y. D. Park, B. R. Bennett, H. D. Cheong, G. Kioseoglou, A. Petrou, *Phys. Rev. B*, **2000**, *62*, 8180.

[17] A. T. Hanbicki, B. T. Jonker, G. Itskos, G. Kioseoglou, A. Petrou, *Appl. Phys. Lett.* **2002**, *80*, 1240.

[18] S. Datta, B. Das, *Appl. Phys. Lett.* **1990**, *56*, 665.

[19] M. Tanaka, S. Sugahara, *IEEE Trans. Electron Devices* **2007**, *54*, 961.

[20] A. Bhattacharya, Z. Baten, T. Frost, *IEEE Photon. Tech. Lett.* **2017**, *29*, 338.

[21] A. Bhattacharya, Md Z. Baten, I. Iorsh, T. Frost, A. Kavokin, P. Bhattacharya, *Phys. Rev. Lett.*, **2017**, *119*, 067701.

[22] A. Song, J. Chen, J. Lan, D. Fu, J. Zhou, Z. Zhong, J. Guo, X. Wu, Y. Wu, X. Li, S. Huang, Z. Wu, J. Kang, *Appl. Phys. Express* **2020**, *13*, 043006.

[23] Y. Wu, X. Wu, Z. Zhong, J. Zhou, J. Chen, J. Guo, A. Song, X. Li, Z. Wu, J. Kang, *Appl. Phys. Express* **2020**, *13*, 123001.

[24] S. Jahangir, F. Doğan, H. Kum, A. Manchon, P. Bhattacharya, *Phys. Rev. B* **2012**, *86*, 035315.

[25] H. Kum, J. Heo, S. Jahangir, A. Banerjee, W. Guo, P. Bhattacharya, *Appl. Phys. Lett.* **2012**, *100*, 182407.

[26] A. Bhattacharya, Md Z. Baten, P. Bhattacharya, *Appl. Phys. Lett.* **2016**, *108*, 042406.

[27] T.-E. Park, Y. H. Park, J.-M. Lee, S. W. Kim, H. G. Park, B.-C. Min, H.-J. Kim, H. C. Koo, H.-J. Choi, S. H. Han, M. Johnson, J. Chang, *Nat. Commun.* **2017**, *8*, 15722.

[28] X. Liu, N. Tang, C. Fang, C. Wan, S Zhang, X. Zhang, H. Guan, Y. Zhang, X. Qian, Y. Ji, W. Ge, X. Han, B. Shen, *RSC Adv.* **2020**, *10*, 12547.

[29] X. Zhang, N. Tang, L. Yang, C. Fang, C. Wan, X. Liu, S. Zhang, Y. Zhang, X. Wang, Y. Lu, W. Ge, X. Han, Bo Shen, *Adv. Funct. Mater.* **2021**, *31*, 2009771.

[30] G. Schmidt, D. Ferrand, L. W. Molenkamp, A. T. Filip, B. J. van Wees, *Phys. Rev. B*, **2000**, *62*, R4790.

[31] A. Fert, H. Jaffrés, *Phys. Rev. B*, **2001**, *64*, 184420.

[32] S. Takahashi, S. Maekawa, *Phys. Rev. B*, **2003**, *67*, 052409.

[33] N. Nishizawa, K. Nishibayashi, H. Munekata, *Proc. Natl. Acad. Sci. USA* **2017**, *114*, 1783.

[34] J. Sinova, I. Žutić, *Nat. Mater.* **2012**, *11*, 368.

[35] P. E. Faria Junior, G. Xu, Y.-F. Chen, G. M. Sipahi, and I. Žutić, *Phys. Rev. B*, **2017**, *95*, 115301.

[36] I. Žutić, G. Xu, M. Lindemann, P. E. F. Junior, J. Lee, V. Labinac, K. Stojšić, G. M. Sipahi, M. R. Hofmann, N. C. Gerhardt, *Solid State Commun.*, **2020**, *316–317*, 113949.

[37] C. Xie, M. Dan, G. Hu, N. Liu, Y. Zhang, *Nano Energy*, **2022**, *96*, 107100.

[38] J-Y. Chen, T.-M. Wong, C.-W. Chang, C.-Y. Dong, Y.-F. Chen, *Nat. Nanotech.*, **2014**, *9*, 845.

[39] R. Farshchi, M. Ramsteiner, J. Herfort, A. Tahraoui, H. T. Grahn, *Appl. Phys. Lett.* **2011**, *98*, 162508.

[40] T. A. Peterson, S. J. Patel, C. C. Geppert, K. D. Christie, A. Rath, D. Pennachio, M. E. Flatté, P. M. Voyles, C. J. Palmstrøm, P. A. Crowell, *Phys. Rev. B* **2016**, *94*, 235309.

[41] M. Yamada, F. Kuroda, M. Tsukahara, S. Yamada, T. Fukushima, K. Sawano, T. Oguchi, K. Hamaya, *NPG Asia Mater.* **2020**, *12*, 47.

[42] K. Hamaya, M. Yamada, *MRS Bull.* **2022**, *47*, 584.

[43] I. Galanakis, P.H. Dederichs, N. Papanikolaou, *Phys. Rev. B* **2002**, *66*, 174429.

[44] S. Wurmehl, G. H. Fecher, H. C. Kandpal, V. Ksenofontov, C. Felser, H.-J. Lin, J. Morais, *Phys. Rev. B* **2005**, *72*, 184434.

[45] K. Inomata, N. Ikeda, N. Tezuka, R. Goto, S. Sugimoto, M. Wojcik, E. Jedryka, *Sci. Technol. Adv. Mater.* **2008**, *9*, 014101.

[46] Y. Sakuraba, M. Hattori, M. Oogane, Y. Ando, H. Kato, A. Sakuma, T. Miyazaki, H. Kubota, *Appl. Phys. Lett.* **2006**, *88*, 192508.

[47] T. Kimura, N. Hashimoto, S. Yamada, M. Miyao, K. Hamaya, *NPG Asia Mater.* **2012**, *4*, e9.

[48] Z. Nedelkoski, B. Kuerbanjiang, S. E. Glover, A. Sanchez, D. Kepaptsoglou, A. Ghasemi, C. W. Burrows, S. Yamada, K. Hamaya, Q. Ramasse, P. Hasnip, T. Hase, G. Bell, A. Hirohata, V. Lazarov, *Sci. Rep.* **2016**, *6*, 37282.

[49] R. Meijers, R. Calarco, N. Kaluza, H. Hardtdegen, M. v. d. Ahe, H. L. Bay, H. Lüth, M. Buchmeier, D.E.Bürgler, *J. Cryst. Growth* **2005**, *283*, 500.

[50] C. Gao, O. Brandt, H.-P. Schönherr, U. Jahn, J. Herfort, B. Jenichen, *Appl. Phys. Lett.* **2009**, *95*, 111906.

[51] J.-Y. Kim, A. Ionescu, R. Mansell, I. Farrer, F. Oehler, C. J. Kinane, J. F. K. Cooper, N.-J. Steinke, S. Langridge, R Stankiewicz, C. J. Humphreys, R. P. Cowburn, S. N. Holmes, C. H. W. Barnes, *J. Appl. Phys.* **2017**, *121*, 043904.

[52] H. D. Li, K. He, M. H. Xie, N. Wang, J. F. Jia, Q. K. Xue, *New J. Phys.* **2010**, *12*, 073007.

[53] S. Fernández-Garrido, K. U. Ubben, J. Herfort, C. Gao, O. Brandt, *Appl. Phys. Lett.* **2012**, *101*, 032404.

[54] S. Yamada, K. Tanikawa, S. Oki, M. Kawano, M. Miyao, K. Hamaya, *Appl. Phys. Lett.* **2014**, *105*, 071601.

[55] Y. Fujita, M. Yamada, M. Tsukahara, T. Oka, S. Yamada, T. Kanashima, K. Sawano, K. Hamaya, *Phys. Rev. Appl.* **2017**, *8*, 014007.

[56] J. Tatebayashi, T. Yamada, T Inaba, D. Timmerman, S. Ichikawa, Y. Fujiwara, *Appl. Phys. Express* **2019**, *12*, 095003.

[57] D. Timmerman, Y. Matsude, Y. Sasaki, S. Ichikawa, J. Tatebayashi, Y. Fujiwara, *Phys. Rev. Appl.* **2020**, *14*, 064059.

[58] T. M. Nakatani, A. Rajanikanth, Z. Gercsi, Y. K. Takahashi, K. Inomata, K. Hono, *J. Appl. Phys.* **2007**, *102*, 033916.

[59] M. Johnson, R. H. Silsbee, *Phys. Rev. Lett.* **1985**, *55*, 1790.

[60] F. J. Jedema, H. B. Heersche, A. T. Filip, J. J. A. Baselmans, B. J. van Wees, *Nature* **2002**, *416*, 713.

[61] X. Lou, C. Adelmann, S. A. Crooker, E. S. Garlid, J. Zhang, K. S. M. Reddy, S. D. Flexner, C. J. Palmstrøm, P. A. Crowell, *Nat. Phys.* **2007**, *3*, 197.

[62] W. E. Carlos, J. A. Freitas Jr., M. Asif Khan, D. T. Olson, J. N. Kuznia, *Phys. Rev. B* **1993**, *48*, 17878.

[63] A. V. Rodina, B. K. Meyer, *Phys. Rev. B* **2001**, *64*, 245209.

[64] W. F. Koehl, M. H. Wong, C. Poblenz, B. Swenson, U. K. Mishra, J. S. Speck, D. D. Awschalom, *Appl. Phys. Lett.* **2009**, *95*, 072110.

[65] J. H. Buß, J. Rudolph, F. Natali, F. Semond, D. Hagele, *Phys. Rev. B* **2010**, *81*, 155216.

[66] J. H. Buß, J. Rudolph, S. Starosielec, A. Schaefer, F. Semond, Y. Cordier, A. D. Wieck, D. Hagele, *Phys. Rev. B* **2011**, *84*, 153202.

[67] M. Yamada, Y. Shiratsuchi, H. Kambe, K. Kudo, S. Yamada, K. Sawano, R. Nakatani, K. Hamaya, *J. Appl. Phys.* **2021**, *129*, 183901.